Research on Engineering Structures & Materials
www.jresm.org
MIM Research Group

Research Article

Predicting the interfacial bond strength between CFRP and lightweight concrete using machine learning techniques

Kamal Alogla [*,a], Sajjad E. Rasheed [b]

College of Engineering, University of Kerbala, Kerbala, Iraq

Article Info

Article History:

Received 28 Apr 2026

Accepted 19 May 2026

Keywords:

Bond-slip behavior;
Lightweight concrete;
CFRP composites;
Artificial neural network;
Genetic algorithm;
Multiple linear regression

Abstract

Among the variables that govern how well a retrofitted concrete member performs in service, few are as consequential as the bond between the substrate and an externally attached strengthening layer. For CFRP (carbon fiber-reinforced polymer) systems in particular, the ultimate failure load recorded in single-lap or double-lap shear tests has long served as the principal measure of this bond capacity, yet reliable predictions still rely almost exclusively on labor-intensive laboratory campaigns or analytical formulas calibrated solely on normal-weight concrete (NWC). In this study, three predictive modelling approaches namely artificial neural network (ANN), multiple linear regression (MLR), and a genetic algorithm (GA)-calibrated power-law empirical formula, were developed and rigorously evaluated for predicting the ultimate failure load (P_u) of CFRP-to-concrete specimens encompassing both NWC and lightweight concrete (LWC) substrates. A compiled experimental database of 234 specimens was assembled from two independent sources, incorporating six input parameters: bond length (L_e), CFRP width (b_e), CFRP laminate thickness (t_e), fiber orientation angle (θ), concrete compressive strength (f'^c), and concrete type. The ANN model with a 100–50 two-hidden-layer architecture achieved the highest predictive accuracy on the independent test set, with R^2 = 0.83, RMSE = 4.47 kN, and MAE = 3.38 kN, and a 5-fold cross-validation R^2 = 0.87 ± 0.06. The GA calibration produced an explicit power-law empirical formula with test R^2 = 0.68, while the MLR model achieved R^2 = 0.55, confirming the insufficiency of linear approaches for this non-linear problem. Doing a one at a time sensitivity analysis with the ANN model, it was possible to pin down the concrete compressive strength as a dominant factor (sensitivity range = 30.1 kN), then the CFRP fiber orientation angle (22.8 kN) and the CFRP width (22.3 kN). These three were basically the most influential parameters on bond strength. For LWC substrates, the predicted bond capacity came out about 12% lower compared to matching NWC specimens. Overall, the results hand practicing structural engineers validated, data driven predictive tools for design and condition evaluation of CFRP retrofitted LWC structures, and they also help close a gap that was still present in the existing literature.

1. Introduction

Externally bonded fiber-reinforced polymer (FRP) composites, over the past three decades, sort of became one of the most used options for the repair, upgrading of deteriorating reinforced concrete (RC) systems. They are often preferred over plain steel plate bonding or section enlargement, mostly because installation can be done with minimal disruption to ongoing, live loading. Inside the FRP world, carbon fiber-reinforced polymer (CFRP) stands out, primarily due to its high tensile strength (usually 2000–4000 MPa), a stiff elastic response, essentially negligible self-weight and also a strong resistance to fatigue cycling as well as corrosive environments [1-5]. In practice the approach shows up across many RC member categories: CFRP wraps and laminates have been

*Corresponding author: kamal.d@uokerbala.edu.iq
[a]orcid.org/0000-0002-0853-5152; [b]https://orcid.org/0000-0001-7182-1920
DOI: http://dx.doi.org/10.17515/resm2026-1642ma0428rs

reported to raise flexural capacity by as much as 100%, and shear capacity by up to 60% when compared to not-strengthened reference specimens [6-9].

Alongside that broader move toward CFRP strengthening, there has also been growing interest in lightweight concrete (LWC). This type is made by swapping the usual dense aggregates with porous natural or manufactured material like expanded clay, shale, or pumice. The big selling point is structural efficiency: because density can drop by about 20–40% compared with normal-weight concrete, you can end up with lighter foundations, longer spans that still work, and reduced seismic inertia loads. These gains are especially visible in multi storey projects and long span bridge decks [10]. The catch is that the fracture behavior is not the same, at all. Since lightweight aggregate grains are naturally porous and weaker, cracks tend to pass through the aggregate itself rather than being forced to detour around it, which is pretty much the reverse of what is seen in dense natural aggregate concrete. As a result, you commonly get lower splitting tensile strength, less fracture energy, and a failure that feels comparatively brittle [4, 11]. Those material characteristics then influence, quite directly, how well an externally bonded CFRP laminate can stick to the concrete surface before any debonding starts.

Whether the substrate is NWC or LWC, the dominant technical worry in CFRP strengthening is early debonding at the laminate–concrete interface, because that stops the fibers from fully mobilizing their tensile capacity. Stress concentrations near the plate ends and around intermediate flexural cracks generate shear and peel type actions, and these can trigger interfacial delamination or even concrete cover separation [12-14]. In both cases, the loss happens in an abrupt way, almost no gradual warning before the load carrying capacity drops. From a design viewpoint this brittleness becomes the key issue: you cannot just approach the failure load conservatively by relying on ductility allowances. Instead, the failure load must be forecast explicitly from the start of any strengthening plan, not later. That expectation has driven a substantial body of experimental and analytical work focused on describing CFRP–concrete shear bond behavior [15].

Over the past three decades, lots of experimental programs all over the world have churned out extensive data on CFRP-to-concrete bond strength via single lap and double lap shear tests [16-18]. On the basis of those datasets, people have put forward empirical and semi-empirical bond strength models, like [1, 17, 19-21]. In general, these models write the ultimate bond force as some kind of function involving concrete compressive strength, CFRP axial stiffness, and bond length, and they often lean on fracture mechanics ideas [22-24]. But still, these analytical models are mostly calibrated using NWC data with unidirectional CFRP laminates, with a 0° orientation, and then their performance drops, sometimes pretty badly when they are moved outside the original calibration zone—like for LWC substrates, off-axis fiber orientations, or multi-layer laminates [17].

Due to those issues, there has been a noticeable shift toward data driven alternatives. Machine learning (ML) approaches are basically not tied to a pre-set functional form, they instead dig out a predictive pattern straight from experimental measurements, which makes them quite suitable for bond problems where several geometry and material factors are interacting at once [25-29]. For FRP-reinforced concrete, the number of studies has risen quickly. In the RC durability setting, and [30] put forward an early argument for ML-based service-life models. Bond strength itself shows up more clearly in [31], where MLR, SVM, and ANN were compared, and they reported SVM was only slightly better, for that particular dataset. After that , work expanded both the type of model and the overall scope :[32] pushed soft computing into FRP bar pull-out ; [33] showed ensemble strategies may beat single learners; [34-37] moved through successively larger comparative efforts , including explicit neural-network equations, code-model benchmarks , ensemble approaches, and multi-algorithm reviews, each in turn. Earlier adjacent efforts, like steel-bar bond [38] and splice-strength prediction [39] had already indicated that ANN can be a dependable option in the RC bond area.

Still, even with that expanding literature, investigations that focus specifically on CFRP-to-LWC bond strength using ML methods are extremely scarce. Most of the available ML models, including those reported by [31, 33, 34, 37] were trained and validated only with NWC data, and none of them includes LWC specimens in the training database. To the authors' knowledge, the experimental campaign of [16] represents one of the very few published datasets that includes both NWC and

LWC specimens tested under otherwise identical conditions, yet no prior ML study has exploited this dataset to build a predictive model that explicitly accounts for concrete type as an input variable. This study addresses this gap directly by: (i) assembling a comprehensive experimental database that explicitly includes LWC specimens alongside NWC data; (ii) implementing and comparing three predictive modelling approaches of increasing complexity (MLR, GA-calibrated empirical formula, and ANN) on this database; (iii) quantifying the relative importance of six design parameters through a systematic sensitivity analysis; and (iv) deriving and validating an explicit GA-calibrated empirical equation that practitioners can apply without specialist software. The six input parameters considered are: bond length (L_e), CFRP width (b_e), CFRP laminate thickness (t_e), fiber orientation angle (θ), concrete compressive strength (f'^c), and concrete type (NWC or LWC). The output is the ultimate failure load P_u (kN).

2. Research Significance

Taken together, the growth in CFRP strengthening of LWC structures and the systematic absence of LWC data from existing ML bond models creates a substantive gap in knowledge. Design standards currently in use, including ACI 440.2R;[40, 41], fib Bulletin 14 [42], and TR55, were calibrated overwhelmingly on NWC test results and therefore do not reflect the lower fracture energy and reduced tensile strength that characterize lightweight aggregate concrete at equivalent compressive strength grades. These differences are well-established experimentally, yet none of the available bond strength formulas adjusts its predictions for concrete type. Practitioners designing CFRP retrofits for LWC members are therefore left with tools that were not built for that substrate, and there is no validated data-driven model to fill the gap.

Furthermore, while several ML-based models exist for CFRP-NWC bond prediction, the dataset of [16] is, to the authors' knowledge, the only published experimental source that tests both NWC and LWC specimens under identical CFRP bonding conditions, and no prior ML study has been trained on a database containing both concrete types. This limits the generalizability of existing models to the LWC context. The present study advances the state of knowledge in four respects. First, a unified database spanning both concrete types, multiple fiber orientations, and a wide range of CFRP geometries is assembled and made available for future research. Second, three modelling approaches representing different paradigms, namely linear statistical (MLR), evolutionary optimization (GA), and deep learning (ANN), are systematically compared, providing insight into the degree to which non-linear modelling is necessary for this problem. Third, the GA calibration yields an explicit closed-form expression that preserves the physical interpretability of the power-law bond model while benefiting from data-driven coefficient optimization. Fourth, a sensitivity analysis using the most accurate model (ANN) provides a rigorous, quantitative ranking of the six input parameters, which can guide both experimental design and engineering practice in the prioritization of design variables.

3. Methodology

The overall methodology that was adopted in this study is shown in Fig. 1, and it comprises six sequential stages: (1) data collection and database compilation. (2) data pre-processing, encoding, normalization and partitioning of the dataset into training and testing subsets 80:20 split; (3) development and training of the MLR, ANN, and GA models. (4) evaluation of model performance by using R^2, RMSE, MAE and 5-fold cross-validation, which was applied to the MLR and ANN models, only. (5) one-at-a-time sensitivity analysis so to rank input parameter importance (6) derivation of conclusions and some practitioner guidance. The full pipeline was implemented using Python 3.11, with scikit-learn (v1.3) for the ANN and MLR part [43], and SciPy's differential evolution solver for the GA calibration [44].

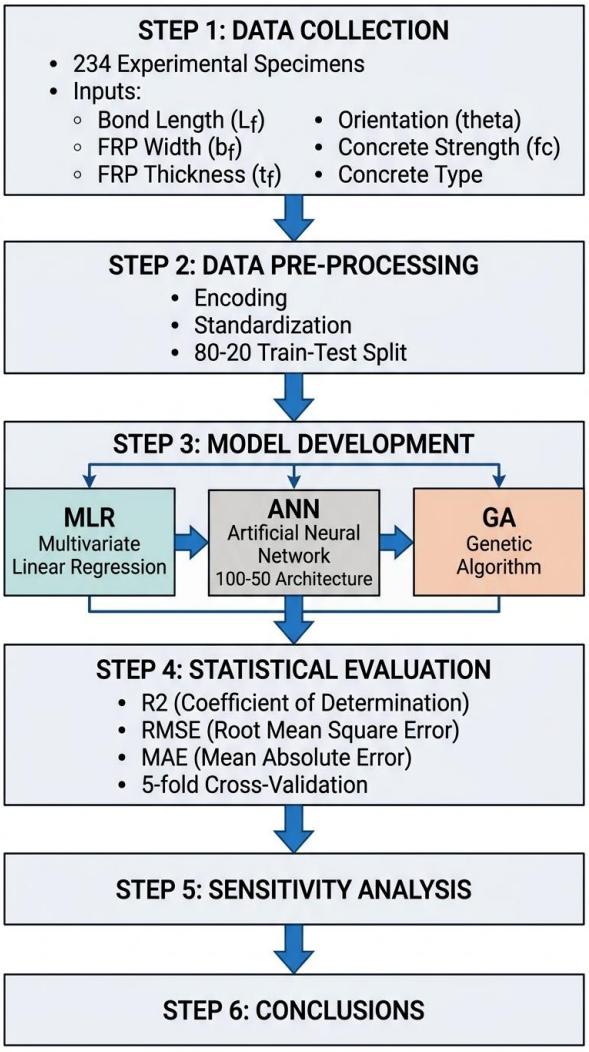

Fig. 1. Flowchart of the methodological framework adopted in this study

3.1. Artificial Neural Network (ANN)

Artificial neural networks (ANNs) were conceived as abstract computational analogues of biological neurons, but in practical engineering they become appealing mostly because of one clean mathematical property: if you use enough width or enough depth, then they can mimic any smooth function, to an arbitrary precision [45]. In the feedforward layout used here, the information goes only in one direction, from the input layer through one or more hidden layers, where non-linear transformations are applied, and finally into one lone output node. At each neuron in layer l, the activation is computed by passing a weighted linear combination of its inputs through a non-linear function [46]:

$$y_j^{(l)} = f\left(\sum_i w_{ij}^{(l)} \cdot y_i^{(l-1)} + b_j^{(l)}\right) \quad (1)$$

where w_{ij} are learnable weights, b_j is the bias, and f is the activation function. In deep multi-layer networks, successive non-linear transformations enable the ANN to approximate arbitrarily complex functions, a capability formalized by the Universal Approximation Theorem [45]. The backpropagation algorithm, combined with first-order gradient methods such as Adam, adjusts all weights and biases iteratively to minimize the mean squared error (MSE) training loss [47].

In this study, a multilayer perceptron regressor (MLPRegressor) was implemented using scikit-learn. The hyperparameter search proceeded in two steps. First, five candidate architectures were evaluated via 5-fold cross-validation: a single hidden layer with 50 neurons (50), a single layer with

100 neurons (100), a two-layer architecture (50–25), a two-layer architecture (100–50), and a three-layer architecture (100–50–25). The architecture (100–50) yielded the highest mean cross-validation R^2 and was selected as the final model. Second, the L^2 regularization parameter α was tuned over the grid using {0.0001, 0.001, 0.01, 0.1} 5-fold cross-validation on the training set; α = 0.001 achieved the best mean CV R^2 and was adopted. The ReLU (rectified linear unit) activation function was used throughout the hidden layers owing to its computational efficiency and its ability to avoid vanishing gradients in multi-layer architectures. The Adam optimizer was used with a fixed initial learning rate of 0.001, L^2 regularization parameter α = 0.001, and a maximum of 2000 iterations. Early stopping was activated with a validation fraction of 10% to prevent overfitting; training was terminated when the validation loss failed to improve by more than 10^{-4} for 10 consecutive iterations. All five continuous input features were standardized to zero mean and unit variance before training; the binary concrete type indicator was retained in its original 0/1 form.

The multilayer perceptron model structure was chosen over ensembles of decision trees (such as Random Forest, XGBoost) due to the continuous differentiability of the input-output relationship required for the smooth one-at-a-time sensitivity curves, as well as the possibility of exporting it as an explicit weight matrix for future use. The small size of the training set (187 samples) was compensated by the L^2 regularization and early stopping methods rather than altering the model class, and future research with large amounts of data might benefit from the comparison of the two classes of models.

3.2. Multiple Linear Regression (MLR)

Contrary to the more complex models, a multiple linear regression (MLR) approach was used to set a performance benchmark and obtain the linear effect of each input on the dependent variable in the form of a regression coefficient [48]. The model can be expressed as follows:

$$P_u = \beta_0 + \beta_1 L_e + \beta_2 b_e + \beta_3 t_e + \beta_4 \theta + \beta_5 f'^c + \beta_6 C + \varepsilon \quad (2)$$

where β_0 is the intercept, β_1–β_6 are the partial regression coefficients associated with each input feature, and ε is the residual error term. The optimal coefficient vector β is determined analytically via ordinary least squares (OLS), which minimizes the residual sum of squares:

$$\beta = (X^T X)^{-1} X^T y \quad (3)$$

where X is the design matrix of standardized input features (including a column of ones for the intercept) and y is the vector of observed failure loads. Although MLR is inherently a linear model and cannot capture interaction terms or non-linear relationships without feature engineering, it is included here for two reasons: (i) as a baseline against which the more complex models can be benchmarked, and (ii) because the resulting coefficient vector provides a direct, interpretable measure of the linear sensitivity of P_u to each standardized input variable.

3.3. Genetic Algorithm (GA) Empirical Model

Unlike gradient-based optimizers, genetic algorithms (GA) maintain a population of candidate solutions and evolve them across successive generations through stochastic selection, crossover, and mutation operators, drawing loose inspiration from Darwinian natural selection. The population is evaluated at each generation using a fitness function; fitter individuals contribute more offspring to the next generation, biasing the population progressively towards the global optimum [49]. For the continuous-parameter calibration problem of this study, the differential evolution (DE) variant [50] was chosen in preference to classical binary-coded GA, because DE operates natively on real-valued vectors and has been shown to converge reliably on civil engineering coefficient-fitting problems without requiring discretization of the search space. The target function chosen for GA calibration is a power-law empirical model inspired by the form of existing analytical bond strength expressions:

$$P_u = a_0 \times L_e^{a_1} \times b_e^{a_2} \times t_e^{a_3} \times (1 + a_4\theta) \times f'^{c_{a_5}} \times (1 + a_6 C) + a_7 \quad (4)$$

where a_0 is a scaling coefficient; a_1–a_3 and a_5 are power-law exponents for the continuous geometric and material variables (L_e, b_e, t_e, and f'^c respectively); a_4 is a linear modifying coefficient for fiber orientation (a power-law form is not appropriate for the $\theta = 0$ case); a_6 is a concrete-type penalty/bonus coefficient; and a_7 is a constant offset. The variable C takes the value 0 for NWC and 1 for LWC. The DE algorithm minimized the mean squared error (MSE) between predicted and experimental P_u over the training set, with a population of 20 individuals per free parameter (160 total), mutation factor F = 0.8, crossover probability Cr = 0.7, and a convergence tolerance of 10^{-6} on the objective function. The algorithm converged after 109 generations.

3.4. Model Evaluation Metrics

All three models were evaluated using three complementary statistical metrics: the coefficient of determination R^2, the root mean squared error (RMSE), and the mean absolute error (MAE). R^2 measures the proportion of variance in P_u explained by the model and ranges from 0 (no predictive ability) to 1 (perfect prediction). RMSE and MAE both quantify average prediction error in kN; RMSE penalizes large outlier errors more heavily than MAE, making the two metrics complementary. The standard formulas for these metrics are:

$$R^2 = 1 - \sum(P_i - \hat{P}_i)^2 / \sum(P_i - \bar{P})^2 \quad (5)$$

$$RMSE = \sqrt{[\sum(P_i - \hat{P}_i)^2 / n]} \quad (6)$$

$$MAE = \sum|P_i - \hat{P}_i| / n \quad (7)$$

where P_i is the experimental failure load of specimen i, $\hat{P}_i$ is the model-predicted value, $\bar{P}$ is the mean of all experimental values, and n is the number of specimens in the evaluation set. In addition, 5-fold cross-validation was performed on the training set (187 specimens) to assess generalization performance for the MLR and ANN models (cross-validation was not applied to the GA model owing to the prohibitive computational cost of repeating the differential evolution optimization across multiple resampling folds): the training data were partitioned into five equal folds, and the model was trained on four folds and evaluated on the held-out fold in each iteration. The mean and standard deviation of cross-validation R^2 across the five folds provide an estimate of the model's expected performance on unseen data together with a measure of the stability of that performance.

4. Data Acquisition and Model Development

The experimental database compiled for this study draws on two primary sources. Dataset 1 comprises single-lap shear test (SST) results for NWC-CFRP joints, sourced from thirteen experimental programs documented in [17] and independently cross-verified against the FRP-to-concrete bond database assembled by [51]. The original programs span the period 1997–2010 and include contributions from research groups in Australia, China, the United Kingdom, Japan, and the United States. After filtering for CFRP-only, single-lap configuration specimens with complete records of all six input variables, 179 NWC specimens were retained from Dataset 1. All Dataset 1 specimens had a nominal fiber orientation of 0° (fibers aligned with the loading direction).

Dataset 2 comprises 55 specimens from the experimental campaign of [16], who conducted double-lap shear tests (DST) on both NWC (21 specimens) and LWC (34 specimens) substrates at the University of Portsmouth. This dataset is particularly valuable because it represents one of the very few published studies that systematically investigated the effect of fiber orientation on bond strength in LWC, testing specimens at 0°, 45°, and 90° orientations, as well as multi-layer CFRP systems with 0/0 and 0/90 layer combinations. For multi-layer specimens, the effective orientation angle was computed as the arithmetic mean of the constituent layer angles (0/90 → 45°; 0/0 → 0°). While this is a simplification — a 0/90 laminate retains axial load-carrying capacity in the 0° ply that arithmetic averaging underestimates — only a small number of 0/90 specimens are present in Dataset 2, limiting the impact of this assumption on overall model performance. Concrete compressive strengths for Dataset 2 were taken directly from [16]: 40.1 MPa for LWC and 41.6 MPa for NWC mix designs.

The total number of 234 samples was split randomly into a training set (80%, 187 samples) and an independent test set (20%, 47 samples) by using a fixed random seed to make the procedure reproducible. No explicit stratification based on the type or orientation of concrete was used in the process; by chance, about 7 out of 34 LWC samples (34 × 0.20 ≈ 7) and about 11 out of 55 samples of Al-Allaf et al. were included in the test set. Five numerical inputs (L_e, b_e, t_e, θ, f'^c) were normalized with z-score (μ = 0, σ = 1) based on training data, which was applied consistently to the test data as well to avoid data leakage. The concrete-type binary indicator (C = 0 for NWC, C = 1 for LWC) was kept binary and not normalized with z-score because this transformation would have changed its nature as categorical data. Distributions of each input variable and the target output (failure load) in the whole database are shown in Fig. 2, and the Pearson correlation matrix is shown in Fig.3

Table 1 presents a statistical summary of the combined database. The failure load P_u ranges from 0.47 to 51.78 kN, with a mean of 15.56 kN and a standard deviation of 10.16 kN, indicating substantial variability attributable to the wide range of geometries and concrete types represented. Bond length spans 65–700 mm, CFRP width 25–150 mm, and CFRP laminate thickness 0.11–1.30 mm, covering the practical range of CFRP strengthening applications.

Table 1. Statistical summary of the compiled experimental database (n = 234)

Parameter	Symbol	Min	Max	Mean	Std Dev	Unit
Bond Length	L_e	65	700	199.4	97.6	mm
CFRP Width	b_e	25	150	59.5	24.3	mm
CFRP Thickness	t_e	0.11	1.30	0.324	0.208	mm
Orientation Angle	θ	0	90	11.6	27.4	°
Comp. Strength	f'^c	21.0	65.8	38.7	9.4	MPa
Failure Load	P_u	0.47	51.78	15.56	10.16	kN

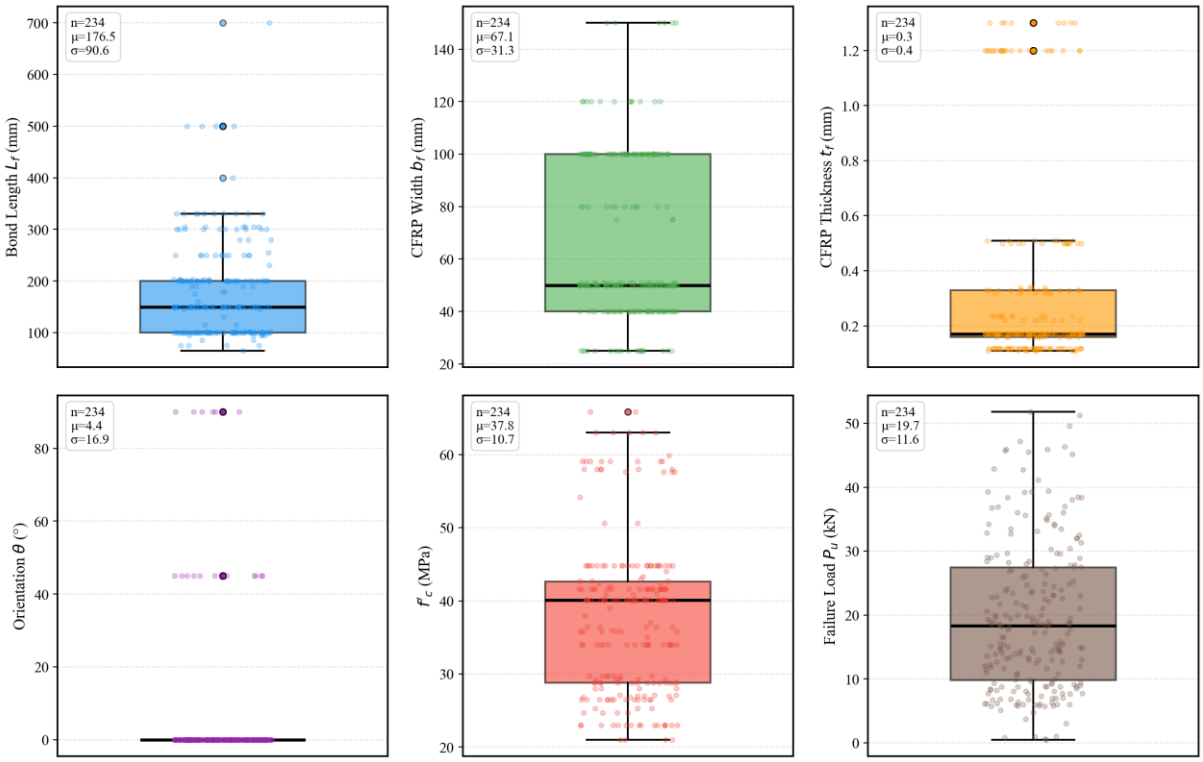

Fig. 2. Distribution of each input parameter and the output failure load P_u across the experimental database (n = 234). Each panel shows the box plot (median, interquartile range, and whiskers) overlaid with individual specimen values (dots)

Fig. 3. Pearson correlation matrix for the six input variables and the output failure load P_u. Values approaching +1 or −1 indicate strong linear association; values near 0 indicate weak or non-linear association

5. Results

5.1. Multiple Linear Regression

The OLS coefficients of the fitted MLR model, expressed in terms of the original un-standardised variables (after back-transformation from the normalised feature space), are presented in Eq. (8). Back-transformation from the standardised coefficients was performed using the training-set means and standard deviations of each feature:

$$P_u = -8.495 + 0.01784\,L_e + 0.2506\,b_e + 14.697\,t_e - 0.2179\theta + 0.1337\,f'^{c} - 5.170C \quad (8)$$

All six coefficients carry the expected physical signs: bond load increases with bond length (0.01784 kN/mm), CFRP width (0.2506 kN/mm), laminate thickness (14.697 kN/mm), and concrete compressive strength (0.1337 kN/MPa), while it decreases with increasing fiber orientation angle (−0.2179 kN/°) and is lower for LWC than for NWC (−5.170 kN). All coefficients are expressed in terms of the original un-standardized variable units (L_e in mm, b_e in mm, t_e in mm, θ in °, f'^{c} in MPa, C binary 0/1), with P_u in kN. The relatively large laminate thickness coefficient (14.697 kN/mm) reflects the strong sensitivity of P_u to t_e over its narrow absolute range in the database (0.11–1.30 mm), consistent with the sub-linear behavior identified in the sensitivity analysis (Section 7).

As a mathematical limitation of the linear model, the negative intercept (−8.495 kN) implies that the model will predict a physically impossible negative failure load when geometric inputs approach zero. Equation (8) should therefore be applied only within the data range for which it was calibrated (Table 1) and should not be used for extrapolation beyond this range.

LWC penalty coefficient (−5.170 kN) is rather high, contributing about 33% to the mean failure load of the database (15.56 kN). Indeed, since the multiple linear regression (MLR) model does not account for interaction effects between input variables, like those between the LWC type and concrete compressive strength and therefore tends to compensate for them too much via the C

coefficient, the effects attributed to it include, in fact, contributions from a number of interacting factors. Sensitivity analysis of the artificial neural network (ANN) model (see Section 7) shows much lower contribution of LWC type (about 2.6 kN or ≈10%) even at the base concrete compressive strength. Thus, the high value of the C coefficient in the MLR model is a consequence of model misspecification rather than the real physical contribution of the parameter in question.

For the training sample, the MLR predicts R^2 = 0.7085, RMSE = 6.32 kN, and MAE = 4.87 kN. For the independent testing sample, these estimates decrease to R^2 = 0.5496, RMSE = 7.23 kN, and MAE = 5.81 kN. For the 5-fold cross-validation, the mean R^2 is 0.6579 ± 0.0721. The ≈15 percentage point difference between training and test R^2 results mainly from systematic under fitting of the linear model to the inherently non-linear CFRP–concrete bond behavior: a model with just six parameters without interaction effects cannot be used to describe multiplicative dependencies between geometric, material, and orientation parameters. The predicted versus experimental scatter is shown in Fig. 4 below. Clearly, the scatter shows systematic underprediction for the high-strength specimens and over prediction for the low-strength ones, resulting from fitting a linear hyperplane to a non-linear function.

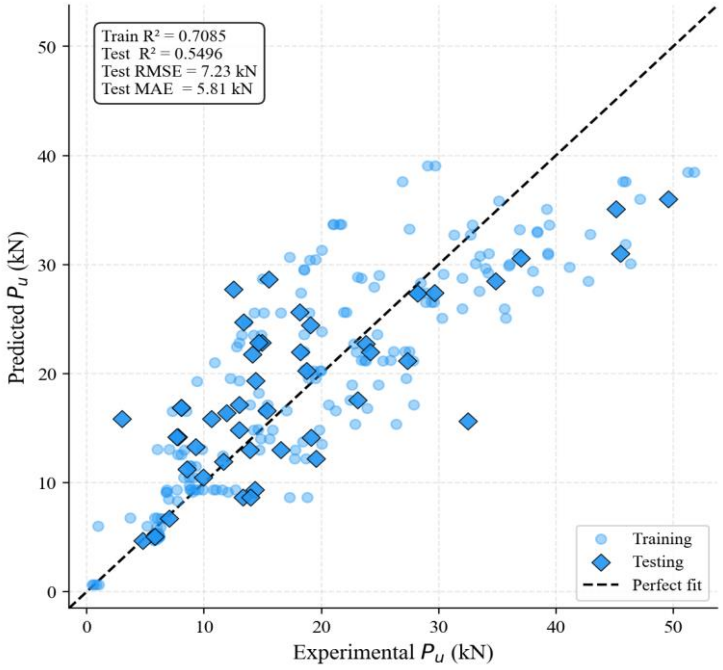

Fig. 4. MLR model: predicted versus experimental failure load P_u. Circles = training specimens; diamonds = test specimens; dashed line = perfect agreement (1:1)

5.2. Artificial Neural Network

In the case of the ANN with the configuration of 100-50, the ANN converged after 567 epochs with early stopping on. The fast convergence shows that the Adam optimizer is effective along with the use of L^2 regularization, as the L^2 regularization prevents the explosion of the weights and thus prevents overfitting. The training performance of ANN was R^2= 0.9118, RMSE=3.48 kN, and MAE=2.70 kN, showing a great enhancement compared to the training performance of MLR. On the independent test set, the ANN attained R^2 = 0.8279, RMSE = 4.47 kN, and MAE = 3.38 kN, representing a 38% reduction in test RMSE relative to MLR. The 5-fold cross-validation yielded R^2 = 0.8653 ± 0.0608, confirming stable generalization with low fold-to-fold variability. Given the model's 5,801 trainable parameters relative to a training set of 187 specimens, the gap between training R^2 (0.91) and test R^2 (0.83) underscores the critical importance of L^2 regularization and early stopping in constraining overfitting; the gap also reflects natural statistical fluctuations in the small test set (47 specimens). The predicted-versus-experimental scatter for the ANN is shown in Fig. 5.

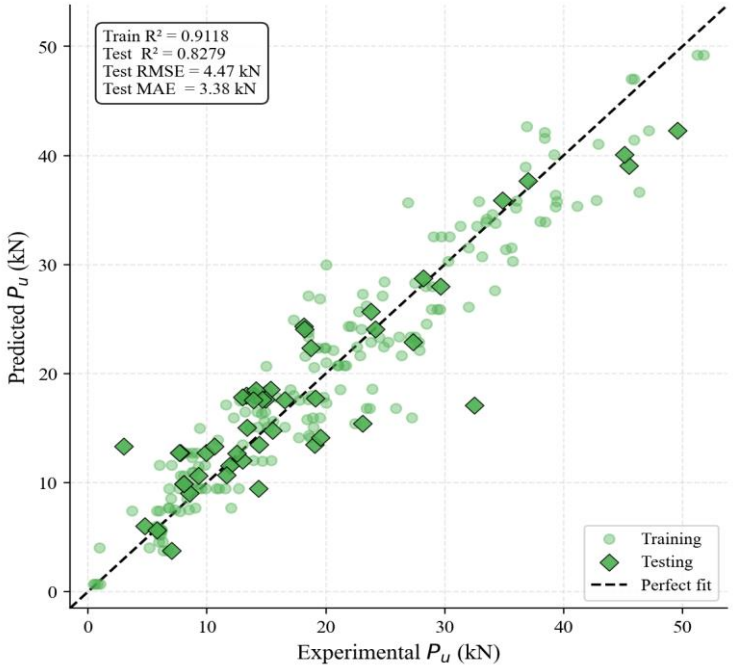

Fig. 5. ANN model (100–50 architecture): predicted versus experimental failure load P_u. Circles = training; diamonds = testing; dashed line = perfect agreement.

5.3. Genetic Algorithm Empirical Model

The differential evolution algorithm converged to the following set of calibrated coefficients for Eq. (4) after 109 generations:

$$P_u = 0.1332 \times L_e^{0.2298} \times b_e^{0.8731} \times t_e^{0.3505} \times (1 - 0.00921\theta) \times f'^{c0.2032} \times (1 - 0.1199C) - 0.5196 \quad (9)$$

In Eq. (9), all length variables (L_e, b_e, t_e) must be expressed in mm, concrete compressive strength f'^c in MPa, and orientation angle θ in degrees; the predicted failure load P_u is then returned in kN. The orientation modifier with its formula (1 − 0.00921θ) reaches zero value at θ ≈ 108.6° and it starts to produce negative values after this point which does not conform to physical laws. The calibration range of the database requires that Eq. (9) be used only for the angle range of θ ≤ 90°.

The physical interpretation of the calibrated exponents is informative. The CFRP width exponent (0.873) is close to unity, confirming a near-proportional relationship between b_e and P_u. Bond length exponent, with the value of 0.230, still stays well below unity, as expected based on the concept of effective bond length [17, 20, 21, 52]. Laminate thickness exponent, being sub-linear with 0.350, considers the effect of CFRP elastic modulus (E_e) variance, as the latter was not included in the analysis due to lack of complete information. Concrete compressive strength exponent of 0.203 suggests an almost f'c^0.2 relationship. Orientation modifier, (1 − 0.00921θ), signifies a decrease in the value of approximately 41% at θ = 45° and 83% at θ = 90°. In particular, it should be mentioned that ANN sensitivity analysis (Section 7) predicts a more pronounced decrease of approximately 52% at θ = 45°, which means that the bond-orientation relationship is nonlinear. The linear modifier in Eq. (9) therefore underestimates the bond capacity decline for strongly off-axis configurations, producing non-conservative (overstated) capacity estimates. Engineers should apply Eq. (9) with caution for off-axis applications (θ > 45°). The LWC penalty factor (1 − 0.1199) equates to a 12% average bond reduction for LWC. The negative constant term (−0.5196 kN) is a mathematical artefact of the regression and indicates that Eq. (9) can yield physically inadmissible negative load estimates at very small geometric values; this confirms that the equation is valid only within the calibrated data range of Table 1.

The GA model achieved training $R^2 = 0.7954$ (RMSE = 5.29 kN) and test $R^2 = 0.6769$ (RMSE = 6.12 kN). Performance is intermediate between MLR and ANN: the power-law form

captures the main non-linear dependencies that the linear MLR model misses, but lacks the representational flexibility of the multi-layer ANN. Unlike MLR and ANN, cross-validation was not performed for the GA model owing to the prohibitive computational cost of repeating the differential evolution optimization across multiple resampling folds; the independent test set therefore serves as the primary generalization estimate for this model. The predicted-versus-experimental scatter is shown in Fig. 6.

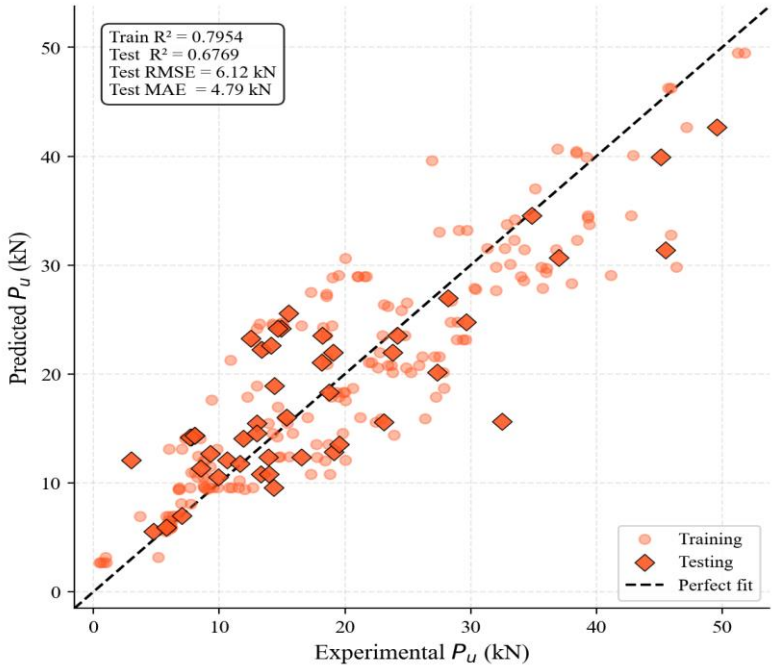

Fig. 6. GA empirical model (Eq. 9): predicted versus experimental failure load P_u. Circles = training; diamonds = testing; dashed line = perfect agreement

6. Results and Discussion

6.1. Comparative Model Performance

Table 2 provides a complete tabulation of performance metrics for all three models. Figs. 7, 8, and 9 present dedicated comparisons of R^2, RMSE, and MAE respectively across training and testing sets. Fig. 10 shows the 5-fold cross-validation R^2 results for the MLR and ANN models; the GA model is excluded from this figure as cross-validation was not performed for it. Taken together, these figures unambiguously establish the ANN as the best-performing model in this study.

The hierarchy in test R^2, with ANN (0.83) > GA (0.68) > MLR (0.55), reflects a consistent ordering in which models with greater representational capacity capture more of the variance in P_u. The improvement from MLR to GA (0.55 to 0.68) demonstrates that the power-law form captures non-linear interactions that linear regression cannot. The further improvement from GA to ANN (0.68 to 0.83) reflects the ANN's ability to learn higher-order interactions and continuous non-linearities.

Table 2. Summary of model performance metrics for training, testing, and 5-fold cross-validation.

Model	Train R^2	Train RMSE (kN)	Train MAE (kN)	Test R^2	Test RMSE (kN)	Test MAE (kN)	CV R^2
MLR	0.7085	6.32	4.87	0.5496	7.23	5.81	0.658 ± 0.072
ANN (100–50)	0.9118	3.48	2.70	0.8279	4.47	3.38	0.865 ± 0.061
GA†	0.7954	5.29	4.07	0.6769	6.12	4.79	N/A

†GA cross-validation was not performed owing to the high computational cost of repeated differential evolution; N/A = not applicable.

In terms of RMSE, the ANN test error of 4.47 kN represents a 38% reduction relative to the MLR test error of 7.23 kN, and a 27% reduction relative to the GA error of 6.12 kN. The coefficient of variation of P_u is 65%, indicating that the ANN's normalized RMSE of 29% represents a substantial reduction from the naive mean predictor. The 5-fold cross-validation R^2 of 0.87 ± 0.06 for the ANN indicates generally stable generalization; however, it should be noted that because the dataset was not stratified, the cross-validation folds may not perfectly balance the representation of LWC and off-axis specimens, and the cross-validation metric may therefore slightly overstate prediction accuracy for these minority classes.

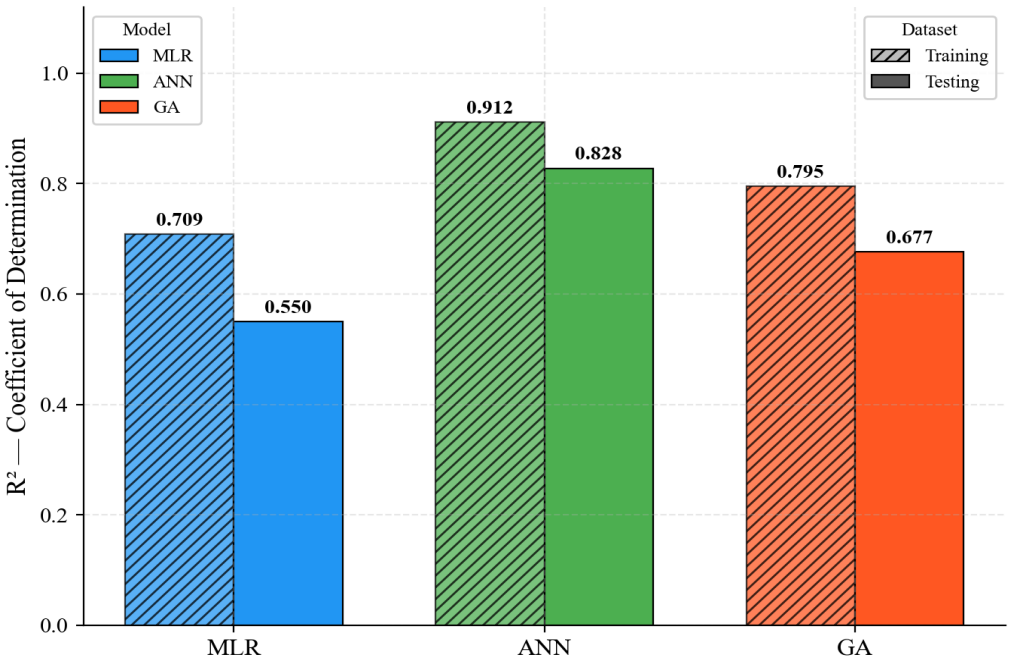

Fig. 7. R^2 comparison for training and testing sets: MLR, ANN, and GA models

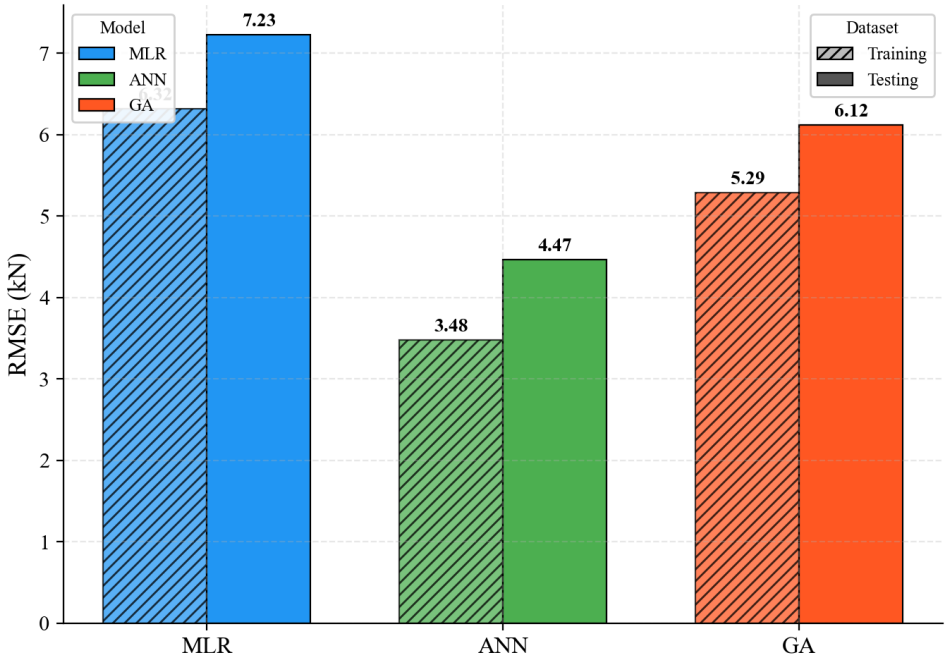

Fig. 8. RMSE (kN) comparison for training and testing sets: MLR, ANN, and GA models

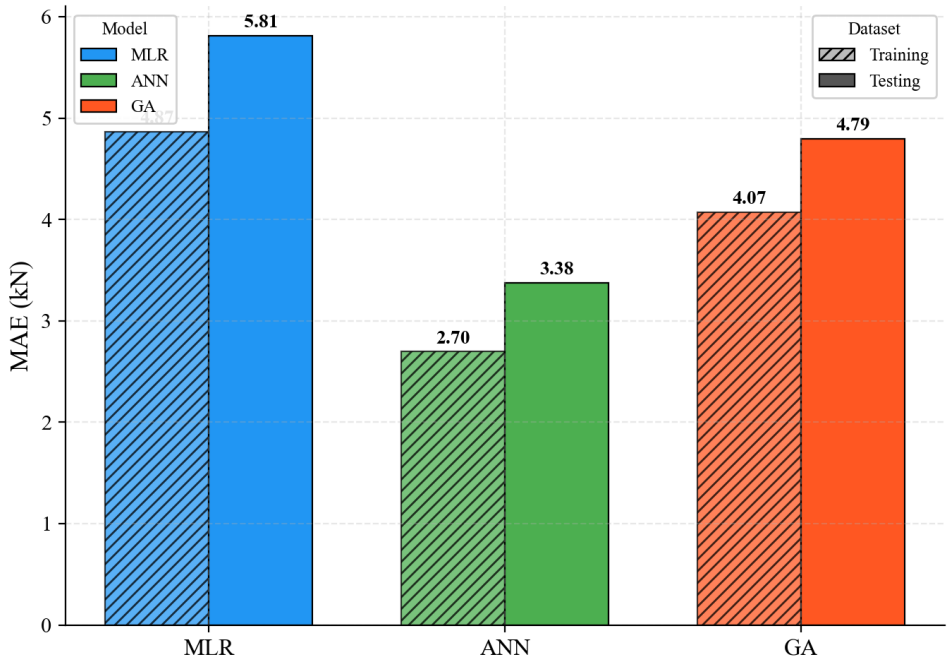

Fig. 9. MAE (kN) comparison for training and testing sets: MLR, ANN, and GA models

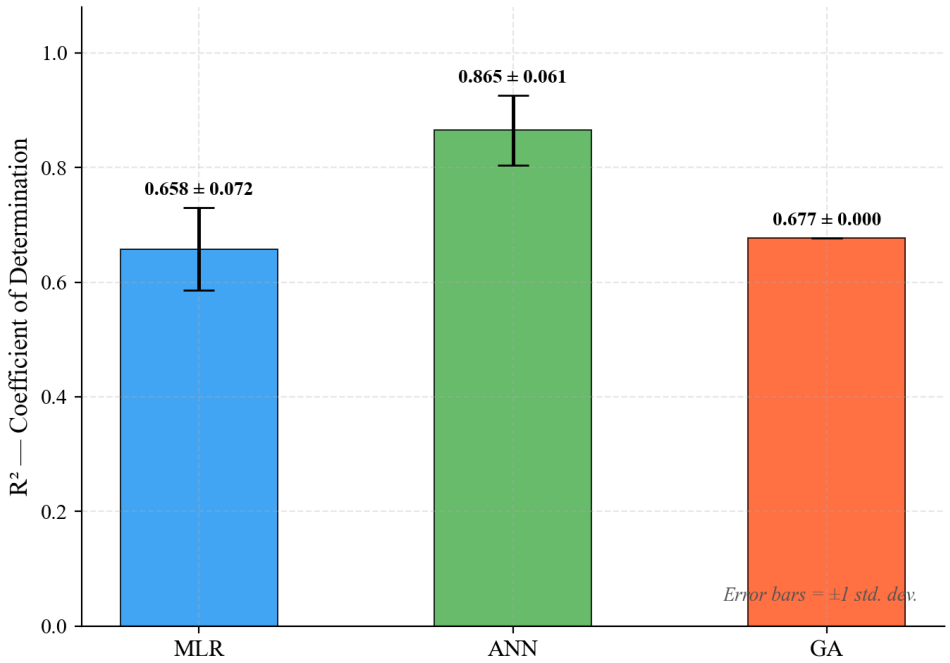

Fig. 10. 5-fold cross-validation R^2 for the MLR and ANN models only. Cross-validation was not performed for the GA model and its result is not included in this figure. Error bars indicate ±1 standard deviation across folds

6.2. Residual Analysis

Figure 11 illustrates the residual analysis for the ANN model. The left plot shows the residuals as a function of the predicted value, whereas the right plot is the residual histogram for both training and test data sets. The residuals are approximately symmetrically distributed around zero for both training and test data sets without any systematic bias depending on the predicted load. The mean value of the test residuals is close to zero, thus the ANN model provides unbiased estimates. The shaded ±RMSE band contains most of the test points, which means that predictions can be considered reasonable in terms of errors. Also, analyzing the residual histogram, it is found that the

residuals follow an approximately normally distributed curve around zero, as expected for a properly fitted model. There is no obvious increase in scatter in dependence on predicted load level, which indicates that the ANN model works equally well throughout the entire range of P_u.

In particular, the homoscedasticity of residuals of the ANN model is interesting in comparison with the results obtained for MLR in Section 5.1. Indeed, if the increased scatter of MLR residuals at high load levels were a characteristic of the data set itself, there should have been a fan-like shape in the ANN residuals plot. As seen in Figure 11, however, the ANN residuals do not depend on the predicted load level. Therefore, the heterogeneity of MLR residuals observed at the extreme load values was caused by linear approximation of the bond mechanism.

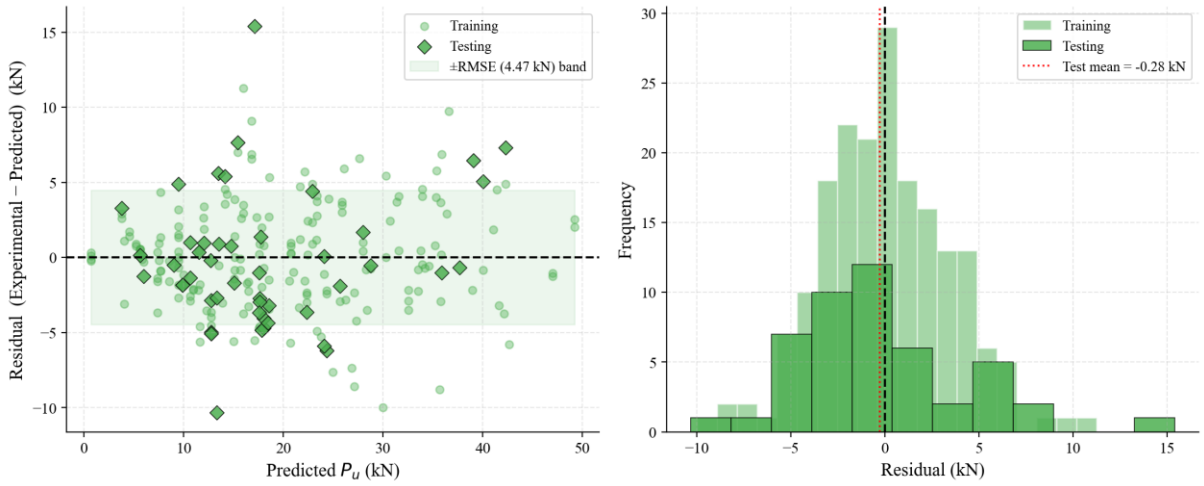

Fig. 11. ANN model residual analysis. Left panel: residuals versus predicted P_u (shaded band = ±RMSE = ±4.47 kN). Right panel: histogram of residuals for training and test sets, with vertical dashed line at zero and dotted line at mean test residual.

6.3. Effect of Concrete Type: LWC versus NWC

A key motivation for this study was to quantify the bond performance difference between LWC and NWC substrates. The GA empirical model (Eq. 9) addresses this directly through the factor (1 − 0.1199C), implying a 12% average bond strength reduction for LWC relative to NWC for identical CFRP geometry and concrete compressive strength. Since all 34 LWC specimens originate from [16], the GA model has learned the LWC penalty directly from that dataset. The 12% factor is therefore best understood as a quantitative formulation of the experimental trend documented by [16], who recorded lower ultimate failure loads and more abrupt, brittle failure modes in LWC specimens compared with NWC counterparts tested under identical conditions, rather than as an independent cross-validation of that finding. The lower fracture energy of LWC, attributable to the weaker aggregate-paste interface and crack propagation through lightweight aggregate particles, reduces the energy available for debonding crack propagation.

The ANN sensitivity analysis (Section 7) places the concrete-type variable last in the importance ranking, with a sensitivity range of 2.62 kN. This outcome is fully consistent with the 12% GA penalty: at the base-point compressive strength of 40 MPa, the difference in predicted P_u between NWC and LWC is 2.6 kN (≈10%), in close agreement with the GA value. The concrete type of variable ranks last in the OAT analysis not because its physical effect is small, but because it is a binary variable that can only take the values 0 and 1, yielding a fixed unit step that is mechanically incomparable to the wide continuous ranges swept by f'^c or b_e. Engineers designing CFRP retrofitting schemes for LWC members should account for both the concrete type and the typically lower tensile strength of LWC relative to NWC at the same nominal compressive strength [10, 53].

6.4. Comparison with Existing Analytical Models

The most widely used analytical bond strength models for FRP-to-concrete, specifically those of [17, 21, 54] were calibrated exclusively on NWC data, with 0° fibre orientation and single-layer

CFRP laminates. When applied to the present database, which includes LWC specimens, off-axis orientations, and multi-layer laminates, they are expected to produce significantly higher errors than reported in their original publications; however, a formal numerical comparison (applying those formulas to the 234-specimen database and computing R^2/RMSE) was outside the scope of the present study and is recommended as a benchmark exercise for future work. Qualitatively, the MLR model (test $R^2 = 0.55$) confirms that linear or semi-empirical approaches with limited input variables are inadequate for the general prediction problem. The GA model ($R^2 = 0.68$) improves upon this, and the ANN ($R^2 = 0.83$) provides the most accurate predictions.

6.5. Limitations

Several limitations of the present study should be acknowledged. First, the target variable is the total failure load P_u (kN) rather than bond stress τ (MPa). Second, CFRP elastic modulus (E_e) was excluded due to incomplete data; its omission may contribute to unexplained variance and partially account for the sub-unity thickness exponent in Eq. (9). Third, the LWC subset comprises 34 specimens from a single program [16] using Lytag lightweight aggregate under controlled laboratory conditions; the trained models may reflect the specific characteristics of this aggregate type and should be applied with caution to LWC produced with different aggregate species (e.g., expanded shale, pumice, aerated concrete) until corroborated by additional data. Fourth, the ANN architecture (100–50) contains 5,801 trainable parameters ($6 \times 100 + 100 \times 50 + 50 \times 1 + 151$ biases) relative to 187 training specimens; L^2 regularization and early stopping substantially mitigate but do not eliminate the overfitting risk from this high parameter-to-sample ratio. Fifth, Dataset 1 (SST, single-lap shear) and Dataset 2 (DST, double-lap shear) employ completely different experimental setups: single-lap joints involve eccentric loading and asymmetric peeling, while double-lap joints have a built-in symmetry. No categoric variable distinguishing between the two tests was considered in the model as an input; such conflation is likely to cause some degree of confounding effect, especially regarding the penalty for LWC, which affects only the DST configuration. Sixth, the GA empirical model (Equation 9) generates negative load predictions when $\theta > 108.6°$ and for very small geometric parameters (due to −0.5196 coefficient); the model equation should be used only within calibrated ranges listed in Table 1. Finally, the random partition proportionally distributed the minority classes (7 of 34 LWC specimens in the test set, consistent with the 20% split ratio), so the marginal difference between CV R^2 (0.87) and test R^2 (0.83) is attributable primarily to the overall small dataset size. Stratified cross-validation in future work with expanded databases would further improve confidence in minority-class predictions.

7. Sensitivity Analysis

A one-at-a-time (OAT) sensitivity analysis was conducted using the trained ANN model to quantify the marginal influence of each input parameter on predicted bond strength. In the OAT approach, each feature is varied across its observed range while all other features are held fixed at a defined base point (L_e = 150 mm, b_e = 100 mm, t_e = 0.17 mm, $\theta = 0°$, f'^c = 40 MPa, NWC). Feature importance is quantified as the sensitivity range, defined as the difference between maximum and minimum predicted P_u over the sweep, in kN. It should be noted that the search of bond length L_e and laminate thickness t_e was performed only for the densest part of the ranges in question (L_e from 65 mm to 300 mm and t_e from 0.11 mm to 0.50 mm, respectively), not the maximums in the database (700 mm and 1.30 mm). Some extremes that lie in the tail of distributions have been excluded to avoid potential artifacts caused by extrapolation. Therefore, the sensitivity ranges that are provided for L_e and t_e can be considered conservative values with their real importance exceeding the given estimates in the whole range.

- Concrete compressive strength (f'^c), Fig. 16: Sensitivity range = 30.14 kN (29.7% of total). The ultimate bond load P_u increases from approximately 4.5 kN at $f'c$ = 21 MPa to 34.6 kN at fc = 65 MPa. This result is in agreement with fracture mechanics models where the failure load of the interface is proportional to the tensile strength of the concrete [17].
- CFRP fibre orientation angle (θ), Figure 15: Sensitivity range = 22.77 kN (22.4% of total). P_u decreases from 26.5 kN at 0° to 12.6 kN at 45° and 3.7 kN at 90° (reductions of 52% and

86%). The ANN predicts a higher reduction at 45° (~52%) than the linear modifier of the genetic algorithm (~41%), indicating that the bond-orientation relationship is nonlinear.

- CFRP width (b_e), Figure 13: Sensitivity range = 22.33 kN (22.0% of total). The bond load increases almost linearly with increasing width from 25 to 150 mm, in line with many analytical models using the linear width factor [21].
- CFRP laminate thickness (t_e), Figure 14: Sensitivity range = 15.40 kN (15.2% of total, swept over 0.11–0.50 mm; the database maximum of 1.30 mm was not swept in full, making this figure a conservative lower bound on t_e's true sensitivity range). P_u increases sublinearly from approximately 22 kN at 0.11 mm to approximately 38 kN at 0.50 mm, as expected from fracture mechanics.
- Bond length (L_e), Figure 12: Sensitivity range = 8.39 kN (8.3% of total, swept over 65–300 mm; the database maximum of 700 mm was not swept in full, making this figure a conservative lower bound on L_e's true sensitivity range). P_u increases from approximately 21 kN at 65 mm to approximately 31 kN at 300 mm, at a strongly decelerating rate, as expected from the idea of an effective bond length.
- Concrete type (NWC/LWC), Fig. 17: Sensitivity range = 2.62 kN (2.6% of total). The ANN predicts P_u = 26.5 kN for NWC and 23.9 kN for LWC (difference 2.6 kN, ≈10%). The small range reflects the binary nature of this variable (fixed 0-to-1 step) rather than a physically small effect; see Section 6.3 for interpretation. Engineers should apply the ANN or GA model with appropriate LWC compressive strength values rather than relying on the binary indicator alone.

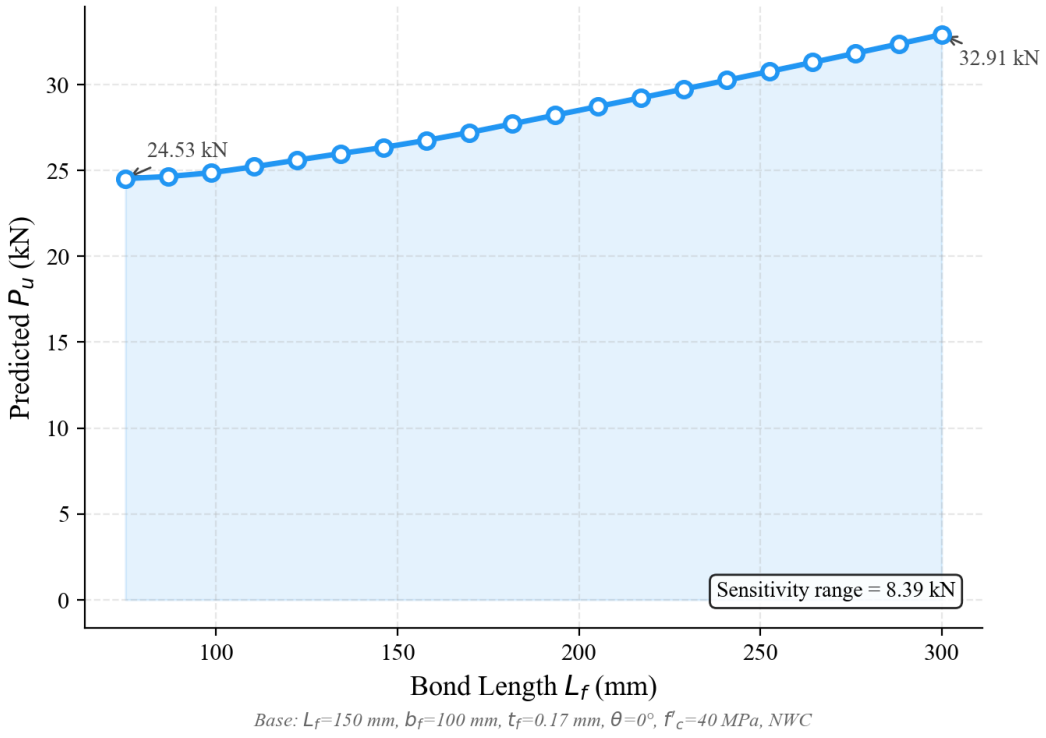

Fig. 12. Sensitivity of predicted P_u to bond length L_e (OAT, sweep 65–300 mm)

Fig. 13. Sensitivity of predicted P_u to CFRP width b_e

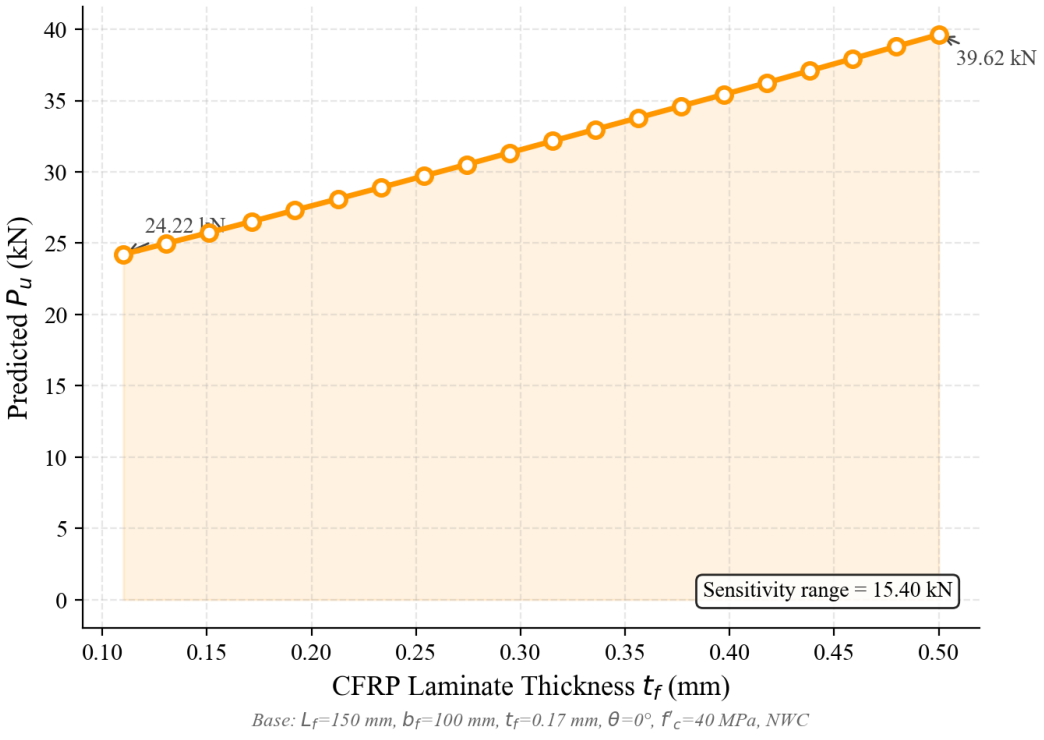

Fig. 14. Sensitivity of predicted P_u to CFRP laminate thickness t_e (sweep 0.11–0.50 mm)

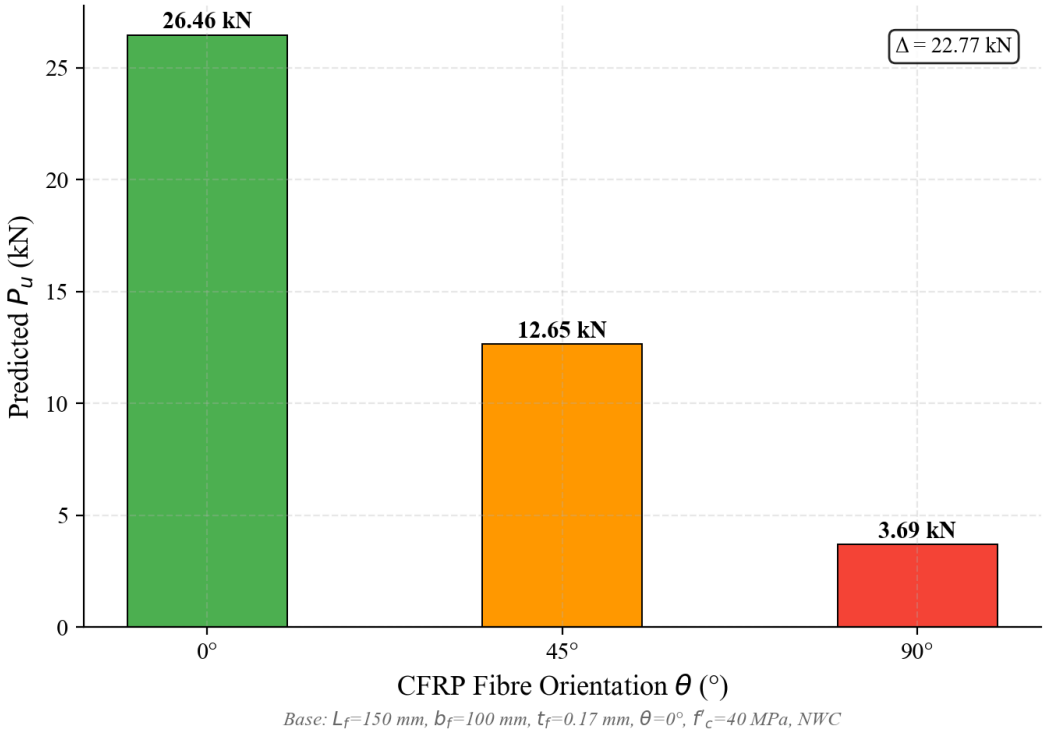

Fig. 15. Sensitivity of predicted P_u to fibre orientation angle θ

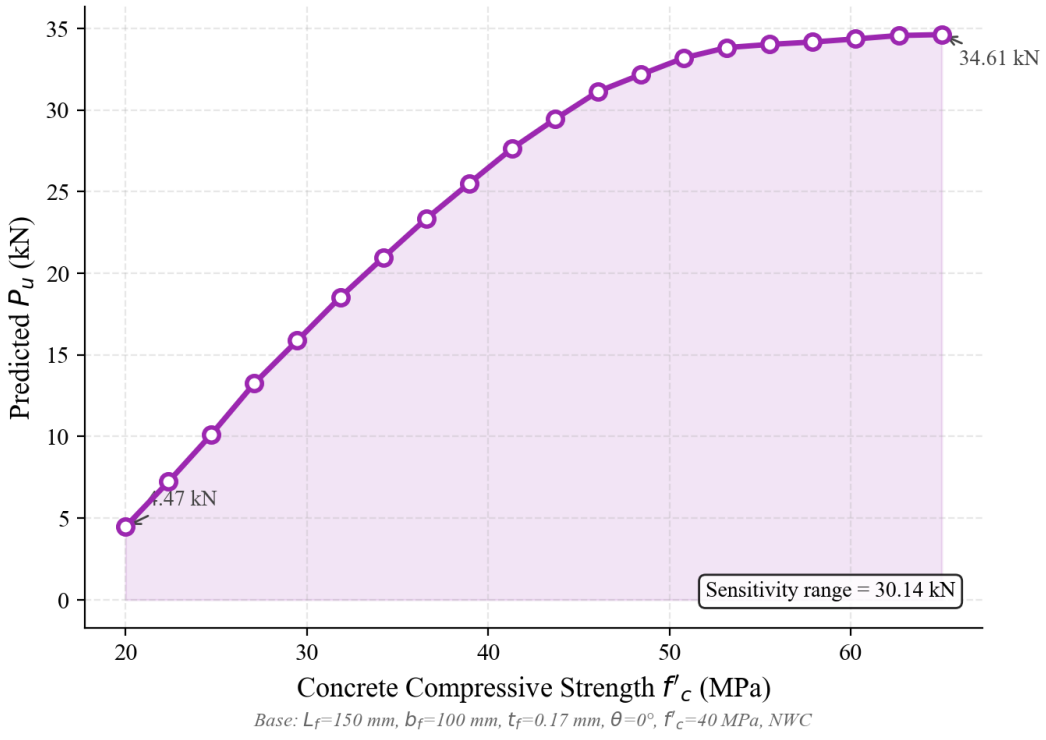

Fig. 16. Sensitivity of predicted P_u to concrete compressive strength f'^c

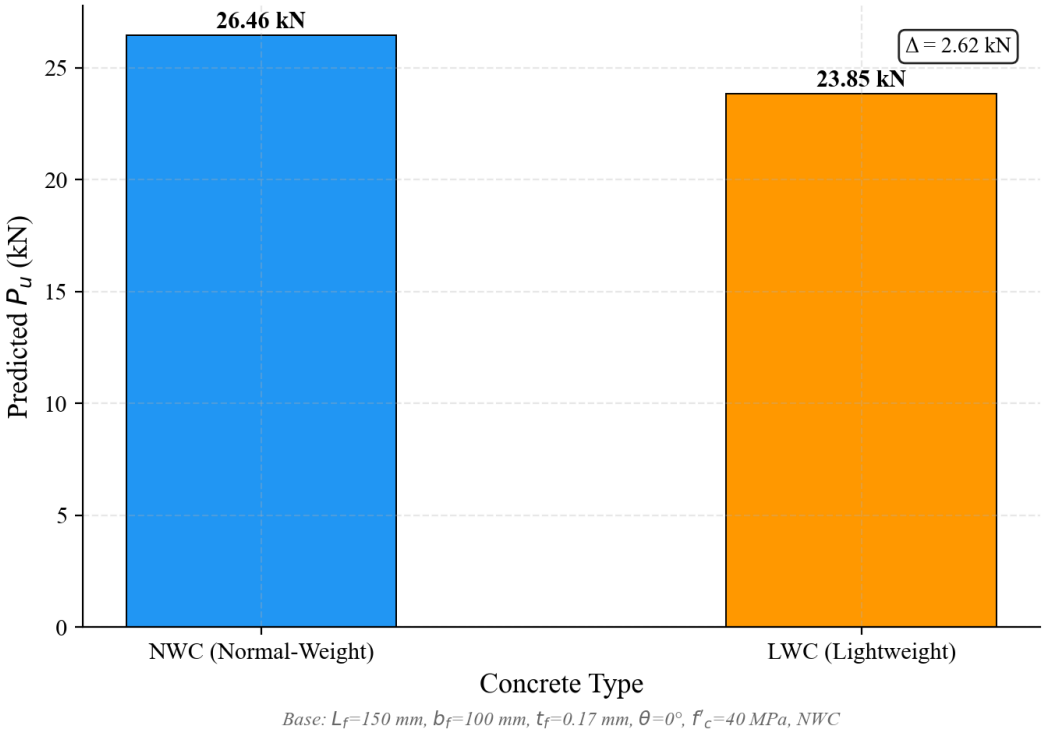

Fig. 17. Sensitivity of predicted P_u to concrete type (NWC versus LWC)

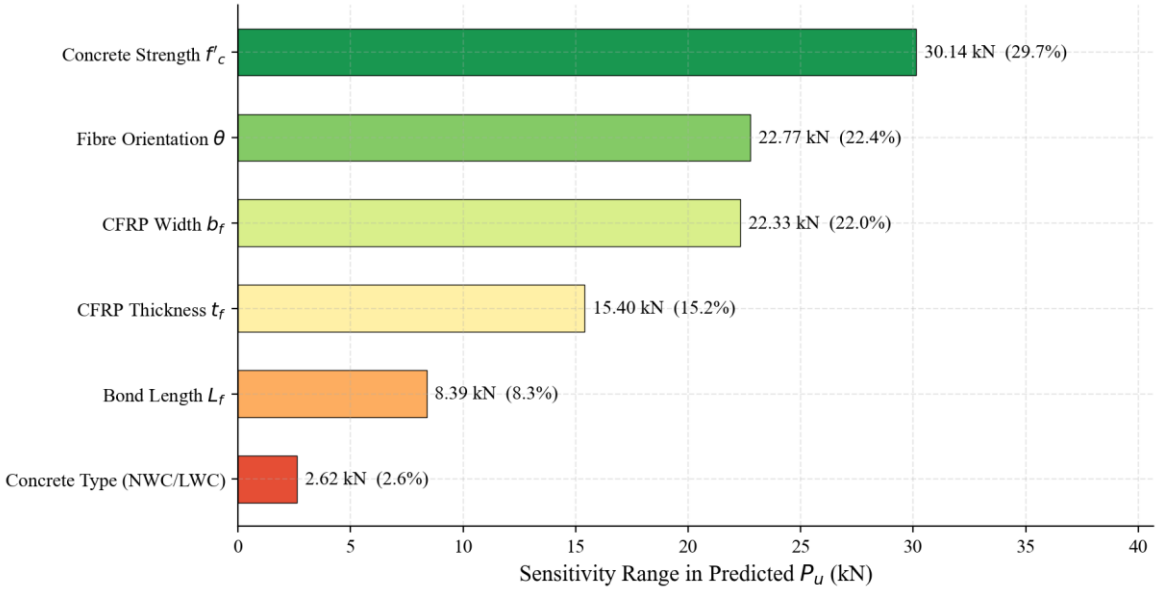

Fig. 18. Feature importance ranking (ANN OAT sensitivity). Note: ranges for L_e and t_e are sub-ranges of the full observed range; their true importance may be higher

8. Conclusions

This study developed, trained, and evaluated three predictive models, namely ANN, MLR, and a GA-calibrated power-law empirical formula, for predicting the ultimate interfacial failure load between CFRP and concrete (both NWC and LWC) using a compiled experimental database of 234 specimens. The following conclusions are drawn:

- The ANN model (100–50) achieved R^2 = 0.83, RMSE = 4.47 kN, MAE = 3.38 kN, and CV R^2 = 0.87 ± 0.06. Residual analysis confirmed unbiased, homoscedastic predictions across the full load range.

- The GA calibration yielded Eq. (9) (test $R^2 = 0.68$) with physically interpretable exponents. Engineers should note that the equation is valid only within the calibrated data ranges of Table 1 and may produce non-conservative estimates for strongly off-axis applications ($\theta > 45°$).
- The MLR model (test $R^2 = 0.55$) confirms linear approaches are insufficient for this problem. The drop between training R^2 (0.71) and test R^2 (0.55) reflects the systematic underfitting that arises when a linear model is applied to a fundamentally non-linear relationship.
- f'^c is the most influential parameter (sensitivity range 30.1 kN, 29.7%), followed by θ and b_e. The low OAT ranking of concrete type arises not from minimal physical significance but from it being a binary variable (0 or 1) with a fixed unit step that cannot be swept across a wide continuous range as f'^c can.
- LWC substrates exhibit ≈12% lower predicted bond capacity than NWC. In practice, the deficit is compounded by LWC's lower tensile strength at the same nominal f'^c. Existing FRP codes, which do not distinguish NWC from LWC, may overestimate achievable bond capacities [10, 53].
- Pending formal code revision, the 12% GA penalty may serve as an interim capacity reduction coefficient applied to ACI 440.2R or fib Bulletin 14 NWC predictions for LWC applications. This recommendation carries the important caveat that the penalty is derived entirely from 34 specimens using Lytag aggregate; it should not be applied to other LWC types (expanded shale, pumice, aerated concrete) without further experimental corroboration. Recommended future extensions: broader LWC database with diverse aggregate types; inclusion of E_e and surface preparation; SST/DST categorical input; and stratified cross-validation.

References

[1] Smith ST, Teng JG. FRP-strengthened RC beams. I: review of debonding strength models. Engineering Structures. 2002;24(4):385-395. https://doi.org/10.1016/S0141-0296(01)00105-5

[2] Teng JG, Zhang JW, Smith ST, et al. FRP-Strengthened RC Structures. Chichester: John Wiley & Sons; 2002.

[3] Zhou Y, et al. Shear strength components of adjustable hybrid bonded CFRP shear-strengthened RC beams. Composites Part B: Engineering. 2019;163:36-51. https://doi.org/10.1016/j.compositesb.2018.11.020

[4] Hosen MA, et al. Structural performance of lightweight concrete beams strengthened with side-externally bonded reinforcement (S-EBR) technique using CFRP. Composite Structures. 2019;210:930-940. https://doi.org/10.1016/j.compositesb.2019.107323

[5] Al-Rousan RZ. Behavior of macro synthetic fiber concrete beams strengthened with different CFRP composite configurations. Journal of Building Engineering. 2019;25:100771. https://doi.org/10.1016/j.jobe.2018.09.009

[6] Khalifa A, et al. Contribution of externally bonded FRP to shear capacity of RC flexural members. Journal of Composites for Construction. 1998;2(4):195-202. https://doi.org/10.1061/(ASCE)1090-0268(1998)2:4(195

[7] Chen C, et al. Mechanism of surface preparation on FRP-concrete bond performance: a quantitative study. Composites Part B: Engineering. 2019;163:193-205. https://doi.org/10.1016/j.compositesb.2018.11.027

[8] Nayak A, Kumari A, Swain R. Strengthening of RC beams using externally bonded fibre reinforced polymer composites. In: Structures. Amsterdam: Elsevier; 2018. p. 28-40. https://doi.org/10.1016/j.istruc.2018.03.004

[9] Al-Rousan R, Haddad R, Al-Halboni A. Bond-slip behaviour between self-compacting concrete and carbon-fibre-reinforced polymer sheets. Magazine of Concrete Research. 2016;68(13):678-695. https://doi.org/10.1680/jmacr.15.00143

[10] Lo TY, WC Tang, Cui HZ. The effects of aggregate properties on lightweight concrete. Building and Environment. 2007;42(8):3025-3029. https://doi.org/10.1016/j.buildenv.2005.06.031

[11] Neville AM. Properties of Concrete. London: Pearson Education; 2011.

[12] Zhang SS, Yu T, Chen GM. Reinforced concrete beams strengthened in flexure with near-surface mounted (NSM) CFRP strips: current status and research needs. Composites Part B: Engineering. 2018;131:30-42. https://doi.org/10.1016/j.compositesb.2017.07.072

[13] Ghorbani M, Mostofinejad D, Hosseini A. Experimental investigation into bond behavior of FRP-to-concrete under mixed-mode I/II loading. Construction and Building Materials. 2017;132:303-312. https://doi.org/10.1016/j.conbuildmat.2016.11.057
[14] Teng JG, et al. Intermediate crack-induced debonding in RC beams and slabs. Construction and Building Materials. 2003;17(6):447-462. https://doi.org/10.1016/S0950-0618(03)00043-6
[15] Mertoğlu Ç, Anil Ö, Durucan C. Bond slip behavior of anchored CFRP strips on concrete surfaces. Construction and Building Materials. 2016;106:518-528. https://doi.org/10.1016/j.conbuildmat.2016.07.060
[16] Al-Allaf MH, et al. An experimental investigation into the bond-slip behaviour between CFRP composite and lightweight concrete. Construction and Building Materials. 2016;113:15-27. https://doi.org/10.1016/j.conbuildmat.2016.03.032
[17] Wu Y, et al. On shear bond strength of FRP-concrete structures. Engineering Structures. 2010;32(3):897-905. https://doi.org/10.1016/j.engstruct.2009.12.017
[18] Yao J, Teng JG, Chen JF. Experimental study on FRP-to-concrete bonded joints. Composites Part B: Engineering. 2005;36(2):99-113. https://doi.org/10.1016/j.compositesb.2004.06.001
[19] Chen JF, Teng JG. Anchorage strength models for FRP and steel plates bonded to concrete. Journal of Structural Engineering. 2001;127(7):784-791. https://doi.org/10.1061/(ASCE)0733-9445(2001)127:7(784
[20] Lu XZ, et al. Bond-slip models for FRP sheets/plates bonded to concrete. Engineering Structures. 2005;27(6):920-937. https://doi.org/10.1016/j.engstruct.2005.01.014
[21] Seracino R, Raizal Saifulnaz MR, Oehlers DJ. Generic debonding resistance of EB and NSM plate-to-concrete joints. Journal of Composites for Construction. 2007;11(1):62-70. https://doi.org/10.1061/(ASCE)1090-0268(2007)11:1(62
[22] Sayed-Ahmed EY, Bakay R, Shrive NG. Bond strength of FRP laminates to concrete: state-of-the-art review. Electronic Journal of Structural Engineering. 2009;9:45-61. https://doi.org/10.56748/ejse.9117
[23] Karzad AS, et al. Repair and strengthening of shear-deficient reinforced concrete beams using carbon fiber reinforced polymer. Composite Structures. 2018;187:101-113. https://doi.org/10.1016/j.compstruct.2019.110963
[24] Zhou YW, Wu YF. General model for constitutive relationships of concrete and its composite structures. Composite Structures. 2012;94(2):580-592. https://doi.org/10.1016/j.compstruct.2011.08.022
[25] Armaghani DJ, Asteris PG. A comparative study of ANN and ANFIS models for the prediction of cement-based mortar materials compressive strength. Neural Computing and Applications. 2021;33(9):4501-4532. https://doi.org/10.1007/s00521-020-05244-4
[26] Ly HB, et al. Estimation of axial load-carrying capacity of concrete-filled steel tubes using surrogate models. Neural Computing and Applications. 2020;33:3437-3458. https://doi.org/10.1007/s00521-020-05214-w
[27] Huang J, et al. A new auto-tuning model for predicting rock fragmentation: a cat swarm optimization algorithm. Engineering with Computers. 2020;37:2729-2743.
[28] Pham BT, et al. Prediction of shear strength of soft soil using machine learning methods. CATENA. 2018;166:181-191. https://doi.org/10.1016/j.catena.2018.04.004
[29] Hoang ND. Estimating punching shear capacity of steel fibre reinforced concrete slabs using sequential piecewise multiple linear regression and artificial neural network. Measurement. 2019;137:58-70. https://doi.org/10.1016/j.measurement.2019.01.035
[30] Taffese WZ, Sistonen E. Machine learning for durability and service-life assessment of reinforced concrete structures: recent advances and future directions. Automation in Construction. 2017;77:1-14. https://doi.org/10.1016/j.autcon.2017.01.016
[31] Su M, et al. Selected machine learning approaches for predicting the interfacial bond strength between FRPs and concrete. Construction and Building Materials. 2021;270:121456. https://doi.org/10.1016/j.conbuildmat.2020.121456
[32] Al-Hamd RKS, et al. An optimized prediction of FRP bars in concrete bond strength employing soft computing techniques. Journal of Building Engineering. 2024;86:108883. https://doi.org/10.1016/j.jobe.2024.108883
[33] Kim B, Lee DE, Kim KK. Ensemble machine learning-based approach for predicting of FRP-concrete interfacial bonding. Mathematics. 2022;10(2):231. https://doi.org/10.3390/math10020231
[34] Zhou Y, et al. Explicit neural network model for predicting FRP-concrete interfacial bond strength based on a large database. Composite Structures. 2020;240:111998. https://doi.org/10.1016/j.compstruct.2020.111998
[35] Basaran B, et al. Estimation of the FRP-concrete bond strength with code formulations and machine learning algorithms. Composite Structures. 2021;268:113972. https://doi.org/10.1016/j.compstruct.2021.113972

[36] Chen SZ, et al. Ensemble learning based approach for FRP-concrete bond strength prediction. Construction and Building Materials. 2021;302:124230. https://doi.org/10.1016/j.conbuildmat.2021.124230
[37] Zhang F, et al. Prediction of FRP-concrete interfacial bond strength based on machine learning. Engineering Structures. 2023;274:115156. https://doi.org/10.1016/j.engstruct.2022.115156
[38] Dahou Z, et al. Artificial neural network model for steel-concrete bond prediction. Engineering Structures. 2009;31(8):1724-1733. https://doi.org/10.1016/j.engstruct.2009.02.010
[39] Golafshani EM, Rahai A, Sebt MH. Prediction of bond strength of spliced steel bars in concrete using artificial neural network and fuzzy logic. Construction and Building Materials. 2012;36:411-418. https://doi.org/10.1016/j.conbuildmat.2012.04.046
[40] Soudki K, Alkhrdaji T. Guide for the Design and Construction of Externally Bonded FRP Systems for Strengthening Concrete Structures (ACI 440.2R-02). In: Structures Congress 2005. 2012. p. 1-8. https://doi.org/10.1061/40753(171)159
[41] Nanni A. North American design guidelines for concrete reinforcement and strengthening using FRP: principles, applications and unresolved issues. Construction and Building Materials. 2003;17(6-7):439-446. https://doi.org/10.1016/S0950-0618(03)00042-4
[42] International Federation for Structural Concrete (fib). Externally Bonded FRP Reinforcement for RC Structures. fib Bulletin. 2001;14.
[43] Pedregosa F, et al. Scikit-learn: machine learning in Python. Journal of Machine Learning Research. 2011;12:2825-2830.
[44] Virtanen P, et al. SciPy 1.0: fundamental algorithms for scientific computing in Python. Nature Methods. 2020;17(3):261-272. https://doi.org/10.1038/s41592-019-0686-2
[45] Hornik K, Stinchcombe M, White H. Multilayer feedforward networks are universal approximators. Neural Networks. 1989;2(5):359-366. https://doi.org/10.1016/0893-6080(89)90020-8
[46] Yang X, et al. Research and applications of artificial neural network in pavement engineering: A state-of-the-art review. Journal of Traffic and Transportation Engineering (English Edition). 2021;8(6):1000-1021. https://doi.org/10.1016/j.jtte.2021.03.005
[47] Marzouk M, Elhakeem A, Adel K. Artificial neural networks applications in construction and building engineering (1991-2021): Science mapping and visualization. Applied Soft Computing. 2024;152:111174. https://doi.org/10.1016/j.asoc.2023.111174
[48] Mata J. Interpretation of concrete dam behaviour with artificial neural network and multiple linear regression models. Engineering Structures. 2011;33(3):903-910. https://doi.org/10.1016/j.engstruct.2010.12.011
[49] Katoch S, Chauhan SS, Kumar V. A review on genetic algorithm: past, present, and future. Multimedia Tools and Applications. 2021;80(5):8091-8126. https://doi.org/10.1007/s11042-020-10139-6
[50] Storn R, Price K. Differential evolution - a simple and efficient heuristic for global optimization over continuous spaces. Journal of Global Optimization. 1997;11(4):341-359. https://doi.org/10.1023/A:1008202821328
[51] Athawale AP. Analysis and development of a database on FRP-to-concrete bond strength [Master's thesis]. Texas Tech University; 2012.
[52] Täljsten B. Strengthening of concrete prisms using the plate-bonding technique. International Journal of Fracture. 1996;82(3):253-266. https://doi.org/10.1007/BF00013161
[53] Kumar A, et al. Compressive strength prediction of lightweight concrete: machine learning models. Sustainability. 2022;14(4):2404. https://doi.org/10.3390/su14042404
[54] Smith ST, Teng JG. FRP-strengthened RC beams. II: assessment of debonding strength models. Engineering Structures. 2002;24(4):397-417. https://doi.org/10.1016/S0141-0296(01)00106-7